Indian Journal of Chemical Technology
Vol. 25, November 2018, pp. 505-521

Adsorption and photocatalytic degradation behaviours of cationic dye BV16 in ZnO-*Ghezeljeh* nanoclay composite/UV-C system: Equilibrium, kinetic and thermodynamic studies

Zahra Hassanzadeh Siahpoosh* & Majid Soleimani

Department of Chemistry, Imam Khomeini International University (IKIU), Qazvin, Iran.

E-mail: z.hassanzadeh.s@gmail.com

Received 17 November 2016; accepted 25 August 2018

Ghezeljeh montmorillonite nanoclay or "*Geleh-Sar-Shoor*" (means head-washing clay) has been used as a natural adsorbent to photocatalytic decolorization of BV16 dye under UV radiation. The results of XRD, FT-IR, CEC, Specific surface area and Zeta potential of the *Ghezeljeh* clay confirm that montmorillonite is the dominant mineral phase. Based on SEM images, it can be understood that the distance between the plates is in nm level. Adsorption of BV16 on to different clays might inhibit its photodegradation has been investigated. The photocatalytic decolorization of BV16 dye under UV radiation in aqueous ZnO-natural *Ghezeljeh* nanoclay composite suspension compared to the behavior of the dye on *Ghezeljeh* nanoclay, ZnO-*Ghezeljeh* nanoclay (shell-core), Cloisite Na^+ nanoclay, ZnO-Cloisite Na^+nanoclay composite, ZnO-Cloisite Na^+nanoclay (shell-core). The linearity of the plots (R^2) demonstrates that pseudo-second order kinetic model play a significant role in the uptake of the dye. The R^2 values show that the dye removal isotherm using ZnO-natural *Ghezeljeh* nanoclay composite follows the Langmuir isotherm at natural temperature and Dubinin–Radushkevich isotherm at upper temperature. Calculation of ΔG^0, ΔH^0 and ΔS^0 showed that the procedure is feasible, spontaneous and endothermic.

Keywords: Nanoclay, Photocatalytic, ZnO, Kinetic, Thermodynamic, Adsorption

The organic chemicals special dyes from the effluents of tannery, textile mills and other pigments industrial companies are an essential measure in environmental protection. The chief topic related to these organic compounds in great quantities in wastewater is their chemical stability and low biodegradability in water organizations, which are potentially cancer-causing materials to the environment[1]. There are many varied classes of dyes, such as azo, reactive, metal complex, azo metal complex and cationic and anionic dyes. Basic Violet 16 (BV16) is a cationic dye, water soluble and nonvolatile. It is ordinarily used in textile, leather activities, in making carbon paper, bull pen, stamp pad inks and paints. BV16 directly injuries skin, eyes, gastrointestinal and breathing region. Its carcinogenicity, generative and increasing harmfulness, neurotoxicity and chronic toxicity towards hominids and animals have also been experimentally established[2]. Numerous chemical and physical procedures, such as exclusion by adsorption on activated carbon, coagulation, electrocoagulation, chemical precipitation and separation of pollutants, etc. are applied for color elimination from textile effluents. One difficulty with these methods is that they are not damaging and chiefly generate pollutant concentrated levels[3]. Advance oxidation processes (AOPs) are progressively used as for the lessening of organic contaminants in a diversity of wastewaters from different manufacturing plants. The benefit of AOPs is the change of organic compounds to less lethal molecules. In perfect situations, it is probable to oxidize the organic molecules entirely to CO_2 and H_2O[4-6]. AOPs were based on the generation of very reactive types such as hydroxyl radicals that oxidize a broad series of chemicals hastily and non-selectively decolorization of dyes. When the semiconductor particles such as ZnO are irradiated with UV-light, an electron promotes from the valence band to the conduction band due to photoexcitation, thus leaving an electron lack or hole in the valence band; in this way, electron/hole couples are created. These electron/hole couples are capable of starting a series of chemical reactions that finally mineralize the contaminants[7]. ZnO is suitable as another photocatalyst for photobleaching of some dyes in bulk and suspension shape, and occasionally showed higher activity than TiO_2[3,8-11]. However, ZnO is unstable in acid conditions and displays hasty

deactivation in bulk use due to aggregation[12]. Formerly, numerous investigators have attempted to prepare ZnO in alloy or composite systems by attaching or impregnating ZnO into a stable inorganic support for example activated carbon, MCM-41, SBA silica, and zeolites[13-17]. Attachment of ZnO in an inorganic support can extend lifecycle and reusability of the photocatalyst[18-20]. Clays represent an attractive substrate for immobilization of variety of photocatalyst. Several researches have reported the application and kinetic study of dye adsorption on many types of clay and their modified shapes. Methylene blue adsorption on clay has been used as a model for cationic dye effluent adsorption[21,22]. Montmorillonite clay mineral has been considered a potential adsorbent toward dyes. In pure shape, montmorillonite exhibits a high ability to adsorb dye particles through a cationic exchange and molecular sieve mechanism[22-24]. Consequences of these investigations recommended that the porous structure and great particular surface capacity of montmorillonite were valuable to photoactivity via improving adsorption, which is the determining stage in the heterogeneous photocatalytic response. Consequently, a combination of adsorption and heterogeneous photocatalysis makes photooxidation further effective for the exclusion of dye compounds from wastewater[20]. Natural clay shows a negative charge of structure which permits it to adsorb positively charged dyes[25.26].

In the present work, *Ghezeljeh* montmorillonite nanoclay as a new natural adsorbent for photooxidation decomposition of cationic dye Basic Violet 16 (BV16) which is broadly used in tannery and textile activities. It is interesting to note at this point that *Ghezeljeh* montmorillonite (*Geleh-Sar-Shoor*) nanoclay ("*Geleh-Sar-Shoor*" means head-washing clay) was used in historic Persia to clean the body, particularly the hair, and to wash dead bodies before funerals. The nanoclay is still used in several areas of Iran. This clay is readily accessible, low-priced (its price is $ 0.1/kg) and environment friendly with chemical and mechanical stability. The *Ghezeljeh* clay is characterized by using Fourier Transform Infrared Spectroscopy (FT-IR), Scanning Electron Microscopy-Energy Dispersive Spectrometer Operating (SEM-EDS), X-ray Diffractometry (XRD), X-ray Fluorescence (XRF), Cation Exchange Capacity (CEC), Zeta potential measurements and specific surface area. The results of XRD, FT-IR, CEC, Zeta potential measurement and specific surface area of the *Ghezeljeh* clay approve that montmorillonite is the main mineral phase. Based on SEM images of the clay, it can be realized that the distance between the plates is in nanometer level. ZnO immobilization[26] into *Ghezeljeh* montmorillonite nanoclay structure and photocatalytic activity nanocomposite in presence of UV light was experienced for cationic dye Basic Violet 16. The effects of operating factorsfor example contact time, primary solution *p*H, primary dye concentration, ionic strength, and solution temperatures on the dye adsorption capacity of ZnO-natural *Ghezeljeh* nanoclay composite was studied. In this study, we consequently investigated whether adsorption of Basic Violet 16 to different clay photocatalysts might prevent its photodegradation. Based on these researches, the isotherm models were used to fit the equilibrium data. Finally, kinetic and thermodynamic of the photocatalytic decomposition process cationic dye were evaluated.

Experimental Section

Methods and materials

Reagents and solutions

All the compounds and reagents used were of analytical mark provided the German company of Merck. Zinc acetate dehydrate, sodium chloride, potassium chloride, potassium iodide, sodium carbonate, ammonia, nitric acid, hexane, ethanol, sodium hydroxide, lithium hydroxide monohydrate and N,N-dimethylformamide (DMF). Since the components were at the highest purity, they were used without any further purification. Commercial cationic dye Basic Violet 16 (BV16) was obtained from Alvan Sabet Co. (Tehran, Iran) used without further purification.The wavelength of maximum absorbance (max) for BV16 is 548 nm. Basic Violet 16 has a molecular weight 368.5 g/mol with chemical formula $C_{23}H_{29}ClN_2$. The dye solutions were produced by diluting a stock solution of 1000 mg/L using 70% doubly distillated water and 30% absolute ethanol by volume. The *p*H of the solutions was checked using *p*H meter and adjusted using 0.1 M HNO_3 and NaOH. The nanoclay (adsorbent) was collected from *Ghezeljeh*, a village 18 km west of the city of *Tafresh* in Iran. Natural Na^+-MMT (Na^+-Cloisitenanoclay) was purchased from Southern Clay Products Co.

Instrumentation

A model 420A digital Orion *p*H meter (Gemini, the Netherlands) equipped with a combined glass

electrode was employed for *p*H adjustments. An ultrasonic water bath (Bandelin, Berlin, Germany) was used to separate and disaggregate clay. X-Ray Diffraction (XRD) data were attained using an Ital Structures diffractometer (GNR, Novara, Italy), with Cu K_α radiation (40 kV/30 mA, λ= 1.542 A°). Fourier Transform Infrared (FT-IR) study was carried out using Tensor Bruker MIR-T27 (Germany) having a standard mid-IR DTGS detector. Philips X-ray fluorescence (XRF) of the sample has been studied using XRF Analysis Instruments (Philips Magix Pro, Netherlands). A scanning electron microscope (SEM) (LEO 1450 VP, Thornwood, N.Y., USA) with variable pressure secondary electron detector and energy dispersive spectrometer operating (EDS) at 30 kV (Oxford INCA software, High Wycombe, U.K.) were used for SEM-EDX analysis. Phillips EM 208 transmission electron microscope (TEM) was used under the operating voltages of 80 kV. Zeta potential measurements were carried out on a Zetameter Zeta CAD (CAD Instruments, France). The specific surface are as were determined with the BET method using a Belsorp mini II instrument (BelJapan, Japan). For recording the UV–visible spectra of dye, during the photodegradation investigate, a Unico (SQ-4802, USA) spectrophotometer was used. To control the reaction temperature, thermostatic circulating water bath Polystat (Cole-Parmer instrument-12101-25, USA) preset at desired temperature. All the experiments were carried out in a 500 mL Pyrex batch photoreactor. The radiation source was a UV-C lamp (125 W, 10 cm length, λ_{max}= 247 nm, manufactured by Arda, Farance), which was placed next a Pyrex 500 mL reactor.

Preparation of the adsorbent

The adsorbent was readied using the *Galehouse*manner[27-31]. Natural nanoclay was first treated by 0.1 M of acetic acid to eliminate carbonates, and then 30% H_2O_2 was used to eliminate mineral and organic impurities. The nanoclay was cautiously washed with doubly distilled water to remove traces of acetic acid and hydrogen peroxide. The treated nanoclay was spread and disaggregated in doubly distilled water through an ultrasonic water bath. The resultant suspension was moved to a measuring cylinder and allowed to stand for 3 h, 26 min, 6 sec for sedimentation. The fine fraction (<2 μm) was removed and then sited in an electric vacuum oven at 50°C for 72 h to be dehydrated. Then, it was placed in a desiccator for following investigation. Scanning electron microscopy (SEM) is an influential technique applied in micro imaging of a diversity of surfaces. Based on SEM images of this clay, it can be understood that the distance between the plates is in nm level (Fig. 1a). Also, the surface morphological structure of *Ghezeljeh* nanoclay at *p*H 2 before and after BV16 dye adsorption was distinguished by SEM (Fig. 2a-b)

Physicochemical characterization of Ghezeljehnanoclay

XRD study

The nanoclay was treated by ethylene glycol, an organic compound which gradually intercalates itself into the lattice of the clay. The structural possessions of the nanoclay were observed before and after treatment by ethylene glycol. The X-Ray diffraction analysis (from 2 to 40º 2θ at room temperature) exposed that the nanoclay sample was essentially composed of montmorillonite minerals (Fig. 1b)[32, 33].

FT-IR study

A FT-IR spectrum was recorded in the range of 400-4000 cm^{-1} using the KBr pellet technique. The FT-IR analysis, too, confirmed that the nanoclay was principally composed of montmorillonite minerals (Fig. 1c)[32-34].

XRF and EDS study

XRF and EDS are the chief analytical apparatuses for defining the elemental composition of trace indication items. Table 1 and Fig. 1d exhibit chemical composition of this nanoclay.

Cation exchange capacity (CEC)

The cation exchange capacity (CEC) is the number of equals of moveable charge per mass of clay, which is corresponding with the layer charge[35]. The CEC of the *Ghezeljeh* montmorillonite nanoclay was evaluated with 0.01 M Cu-triethylentetramine[36, 37]. The CEC value of 160.0 meq/100 g for *Ghezeljeh* montmorillonite nanoclay was calculated, and the very great CEC value approves well with the CEC values for Montmorillonite published in the literature[36].

Surface area

The specific surface area (S_{BET}), pore volume and pore radius of the *Ghezeljeh* montmorillonite nanoclay were derivative from N_2 adsorption isotherms measured at liquid nitrogen temperature (at 77 K) by means of a Belsorp mini II instrument

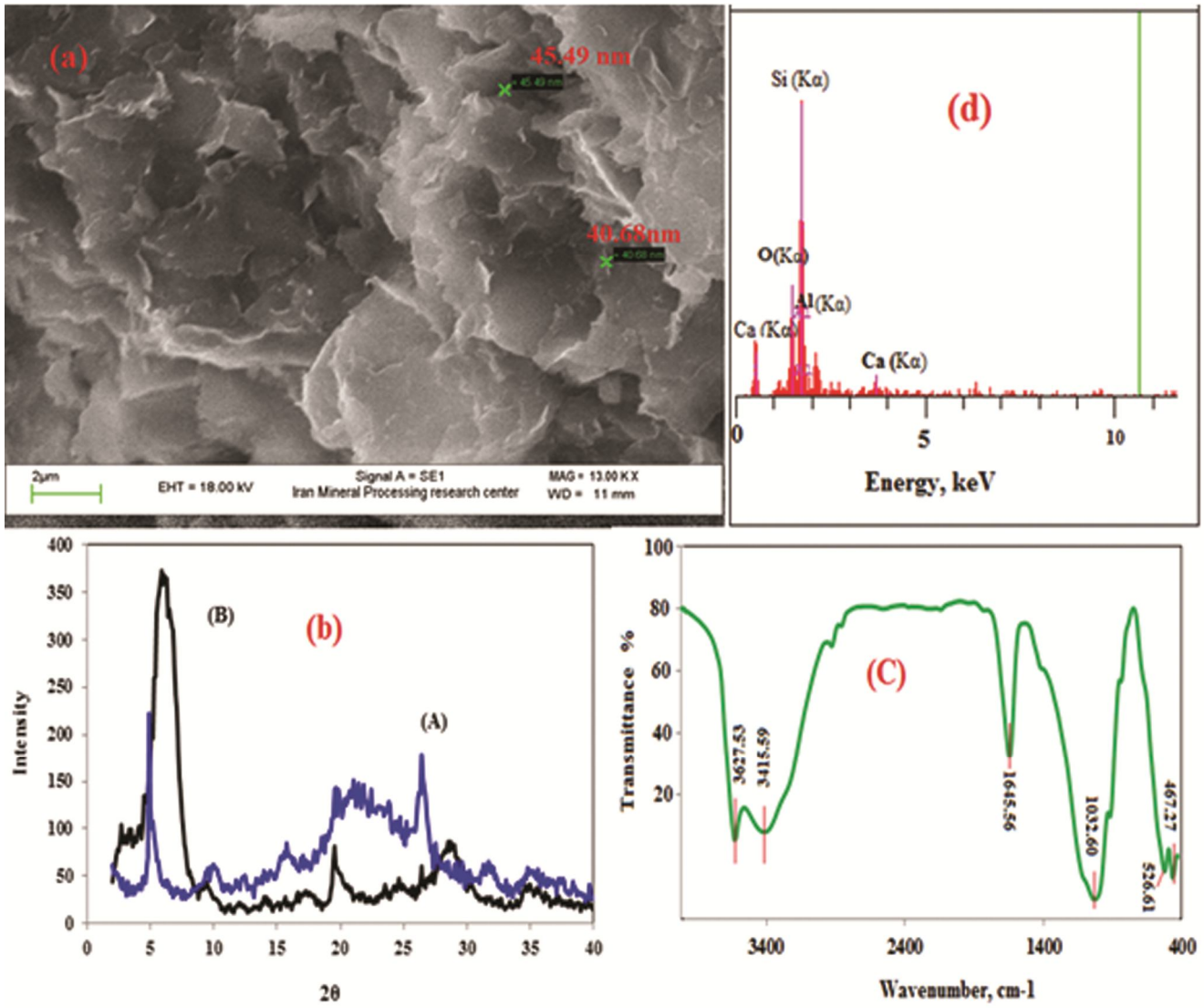

Fig.1 — (a) SEM images (b) XRD patterns of the *Ghezeljeh* nanoclay are treated with ethylene glycol (A), Untreated (B). (c) FT-IR spectrum (d) EDX spectrum of untreated *Ghezeljeh* nanoclay.

(Bel Japan, Japan). Humidity and vapors on the solid surface or entered in the open holes were eliminated by warming under vacuum at 100°C for 12 h previous to the surface area evaluations. The *Ghezeljeh* montmorillonite nanoclay has a specific surface area 90.916 m^2/g, pore volume of 0.147 cm^3/g and pore radius of 4.8 nm[39, 40].

Zeta Potential Measurement

The zeta potential of the Ghezeljeh nanoclay was achieved from electrophoretic mobility measurements at 21.31°C, with Zetameter apparatus (ZetaCAD instruments). The zeta potential measured at a natural *p*H of 5.64 is -25.970 mV and comparable to zeta potentials of montmorillonite (−21.2 mV)[25].

Synthesis of various types of ZnO/clay for comparison photo degradability

Synthesis of ZnO- Ghezeljehnanoclay composite

Nanocomposite was readied by the precipitation manner. 10 g of purified *Ghezeljeh* nanoclay was added to a solution containing 2 g zinc acetate dehydrate dissolved in 250 mL of DMF and the mixture was sonicated for nearly 3 h in order to achieve uniform suspension. To this solution, 100 mL of 0.1 M $NaOH/H_2O$ solution was added dropwise through continuous stirring for 1 h. The nanocomposites powder was attained after succeeding centrifugation and spreading in alcohol and the solid mass was dried at 75°C under vacuum for 4 h and finally, calcinated in air at 200°C for 2–3 h.

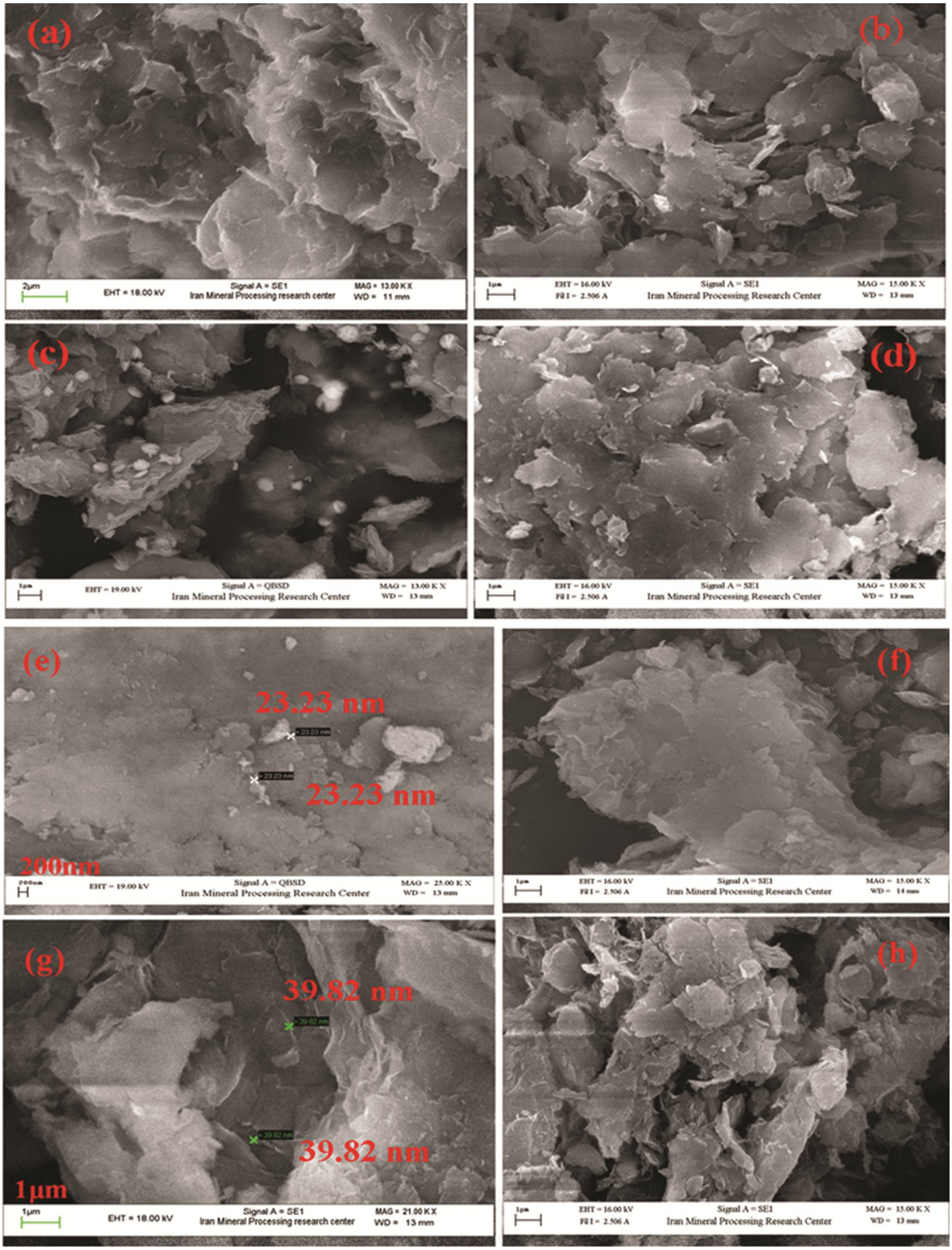

Fig.2 — SEM images of *Ghezeljeh* nanoclay (a) before and (b) after adsorption of BV16, ZnO-*Ghezeljeh*nanoclay composite (c) before and (d) after adsorption of BV16, Nano-ZnO particle supported on *Ghezeljeh* nanoclay (shell-core) (e) before and (f) after adsorption of BV16, Na^+-cloisite nanoclay (g) before and (h) after adsorption of BV16, ZnO-Na^+-cloisite nanoclay composite (i) before and (j) after adsorption of BV16, Nano-ZnO particle supported on Na^+-cloisite nanoclay (shell-core) (k) before and (l) after adsorption of BV16, (m) FT-IR spectrum and (n) EDX spectrum ZnO-*Ghezeljeh* nanoclay composite, TEM images of Nano-ZnO particle supported on *Ghezeljeh* nanoclay (shell-core) (O) before adsorption of BV16. (*Contd*.)

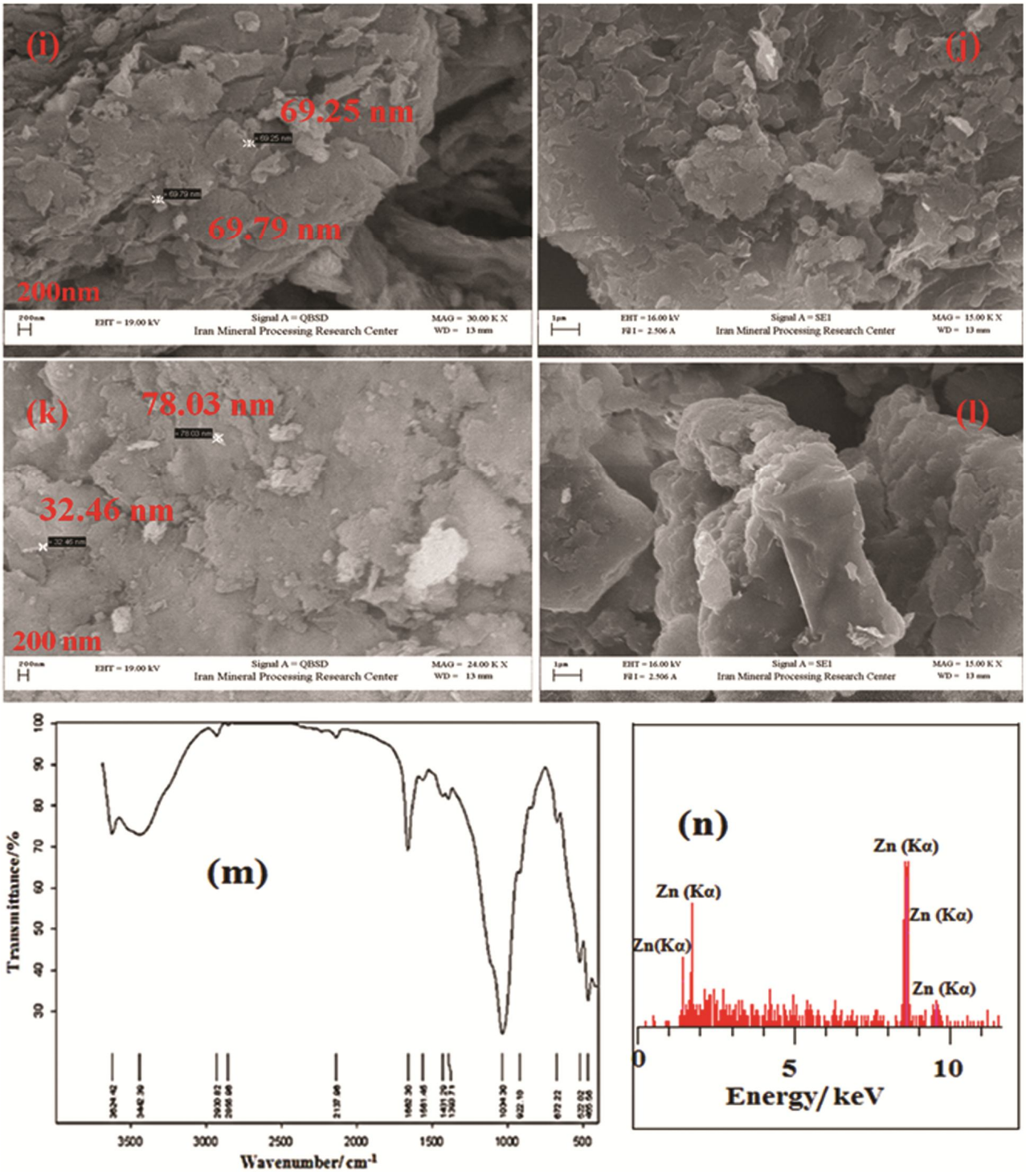

Fig.2 — SEM images of *Ghezeljeh* nanoclay (a) before and (b) after adsorption of BV16, ZnO-*Ghezeljeh*nanoclay composite (c) before and (d) after adsorption of BV16, Nano-ZnO particle supported on *Ghezeljeh* nanoclay (shell-core) (e) before and (f) after adsorption of BV16, Na^+-cloisite nanoclay (g) before and (h) after adsorption of BV16, ZnO-Na^+-cloisite nanoclay composite (i) before and (j) after adsorption of BV16, Nano-ZnO particle supported on Na^+-cloisite nanoclay (shell-core) (k) before and (l) after adsorption of BV16, (m) FT-IR spectrum and (n) EDX spectrum ZnO-*Ghezeljeh* nanoclay composite, TEM images of Nano-ZnO particle supported on *Ghezeljeh* nanoclay (shell-core) (O) before adsorption of BV16. (*Contd*.)

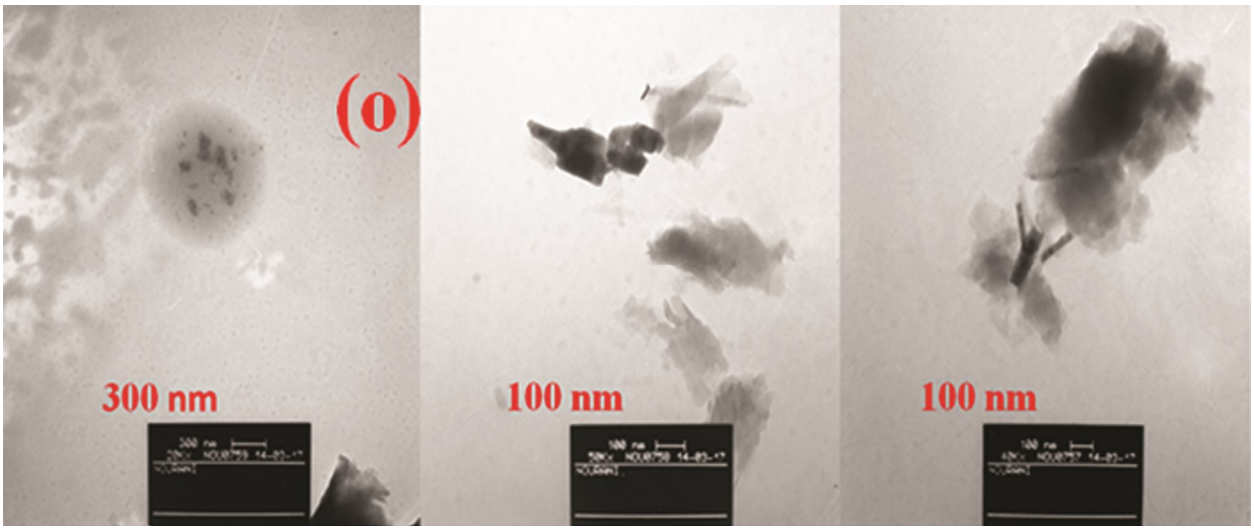

Fig.2 — SEM images of *Ghezeljeh* nanoclay (a) before and (b) after adsorption of BV16, ZnO-*Ghezeljeh*nanoclay composite (c) before and (d) after adsorption of BV16, Nano-ZnO particle supported on *Ghezeljeh* nanoclay (shell-core) (e) before and (f) after adsorption of BV16, Na^+-cloisite nanoclay (g) before and (h) after adsorption of BV16, ZnO-Na^+-cloisite nanoclay composite (i) before and (j) after adsorption of BV16, Nano-ZnO particle supported on Na^+-cloisite nanoclay (shell-core) (k) before and (l) after adsorption of BV16, (m) FT-IR spectrum and (n) EDX spectrum ZnO-*Ghezeljeh* nanoclay composite, TEM images of Nano-ZnO particle supported on *Ghezeljeh* nanoclay (shell-core) (O) before adsorption of BV16.

Table 1 — XRF-analysis of the *Ghezeljeh* Nanoclay

Oxides	%
SiO_2	54.47
Al_2O_3	20.92
MgO	3.65
SO_3	0.32
K_2O	1.82
CaO	1.14
TiO_2	0.37
Fe_2O_3	3.13
PbO	0.16
SrO	0.10
ZrO_2	0.05
As_2O_3	0.02
L.O.I	13.86

The dried ZnO–nanoclay composite was then used for photocatalytic investigation[26]. The surface morphological structure of ZnO-*Ghezeljeh* nanoclay composite at *p*H 2 before and after BV16 dye adsorption was distinguished by SEM (Fig. 2c-d). Furthermore, by using this process, ZnO powder catalyst was synthesized, without any clay.

Synthesis of ZnO particle supported on Ghezeljehnanoclay (shell-core)

ZnO particle supported on *Ghezeljeh* nanoclay (ZnO/*Ghezeljeh*nanoclay) was readied by the sol–gel process using zinc acetate and lithium hydroxide as raw substance and *Ghezeljeh* nanoclay as supporter. 2.2 g $Zn(CH_3COO)_2.2H_2O$ was dissolved in 50 mL anhydrous ethanol at 80°C in an ultrasonic bath. 0.54 g clay was added in solution to make cloudy solution. 0.58 g $LiOH.H_2O$ was dissolved in anhydrous ethanol at room temperature. The hydroxide-containing solution was added to the cloudy solution under strong stirring at 50°C for 60 min. The reaction mixture became ZnO sol which was stayed on the surface of the clay. In excess of twice as much hexane in volume was added to the conical bottle and then the bottle was kept at temperature under 4°C overnight to avoid particles growing swiftly. The white solid would become visible and convert into white gel after being separated from the liquid overhead by a centrifugal machine. The gel was washed by distilled water for the exclusion of the hydrolyzing agent LiOH[25]. The gel was calcined for 4 h at 200°C. The surface morphological structure of ZnO particle supported on *Ghezeljeh* nanoclay (shell-core) at *p*H 2 before and after BV16 dye adsorption was identified by SEM (Fig. 2e-f). TEM images before adsorption of BV16 dye are presented in Fig. 2O. Additionally, by means of this method, ZnO powder catalyst under equal conditions was synthesized, without any clay.

Synthesis of ZnO- Na^+-cloisitenanoclay composite

ZnO-Na^+-cloisite nanoclay composite was synthesized by using the process given in before-mentioned[26]. The surface morphological structure of

Na^+-cloisite nanoclay and ZnO-Na^+-cloisite nanoclay composite at *p*H 2 before and after BV16 dye adsorption were distinguished by SEM (Fig. 2g to 2j)

Synthesis of ZnO particle supported on Na^+-cloisitenanoclay (shell-core)

ZnO particle supported on Na^+-cloisite nanoclay (ZnO/Na^+-cloisite nanoclay) was prepared by using the process given in before-mentioned[25]. The surface morphological structure of ZnO particle supported on Na^+-cloisite nanoclay (shell-core) at *p*H 2 before and after BV16 dye adsorption was identified by SEM (Fig. 2k-l).

The FT-IR spectra of the different clay-based catalysts were recorded at room temperature in the range of 400-4000 cm^{-1} using the KBr pellet technique before and after BV16 dye adsorption, are given in Figs. 2(m) and 3.

Photocatalytic procedures and analysis

Photocatalytic activity of ZnO-*Ghezeljeh* nanoclay composite was evaluated by the degradation of cationic dye Basic Violet 16 as shown schematically in Fig. 4 in a closed box with UV-resistant mirror walls using a Pyrex batch photoreactor with capacity of 500 mL, column shaped in 20 cm height and with an inner and outer diameter of 7 and 9 cm, respectively, under UV light irradiation of a 125 W medium pressure ultraviolet radiation mercuric lamp with a wavelength peak at 247 nm, which was put next the batch photoreactor. The distance between solution and UV source was constant, 5 cm, in all experiments. Heat effect of the lamp during the photoreaction was eliminated by blowing cooled air with two fans between the lamp and the photoreactor. During irradiation, agitation was continued by magnetic stirrer at 750 rpm to keep the suspension uniform. To control the photoreaction temperature, water from the thermostatic bath was circulated to guarantee a constant temperature inside the photoreactor. In order to carry out the experimentations under aerobic conditions, air was driven into the reaction solution by air pump at atmospheric pressure. Photocatalytic activity test achieved at room temperature, photoreactor was charged with 250 mL aqueous solution of BV16 at varying concentrations using doubly distillated water and an identified amount of photocatalyst and was held in a closed box with UV-resistant mirror walls. After addition of the photocatalyst, dye suspension solution was agitated in the dark for 20 min to approve formation of adsorption equilibrium of the dye on catalyst surface. After the start of the reaction by irradiation of the reactor, 5 mL sample of suspension solution were withdrawn a certain time interval and was instantly centrifuged at 3500 rpm for 5 min to entirely take away catalyst particles. The progress of photocatalytic decolorization was monitored by using UV-Vis spectrophotometer at λ_{max} 548 nm. For surveying the effect of the *p*H, the solution *p*H was adjusted initially by adding NaOH or HNO_3.

The efficiency of photodegradation as a function of time is known by:

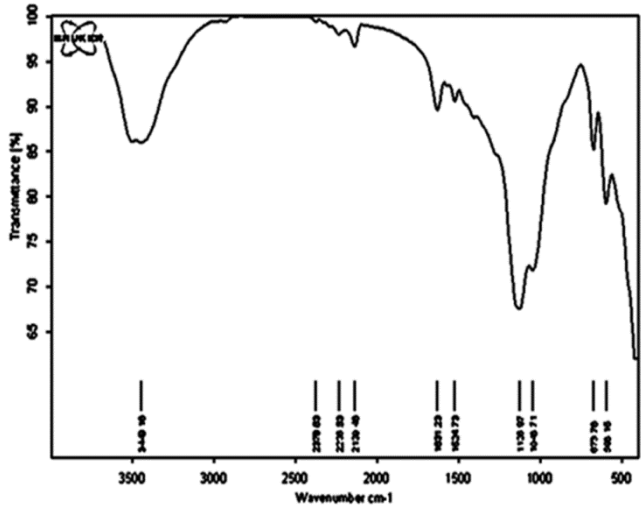

Fig. 3 — FT-IR spectrum of (a) BV16 dye (b)*Ghezeljeh* nanoclay after adsorption of BV16 (c)ZnO-*Ghezeljeh* nanoclay composite after adsorption of BV16, Nano-ZnO particle supported on *Ghezeljeh* nanoclay (shell-core) (d) before and (e) after adsorption of BV16, Na^+-cloisite nanoclay(f) before and (g) after adsorption of BV16, ZnO-Na^+-cloisite nanoclay composite (h) before and (i) after adsorption of BV16, Nano-ZnO particle supported on Na^+-cloisite nanoclay (shell-core) (j) before and (k) after adsorption of BV16.

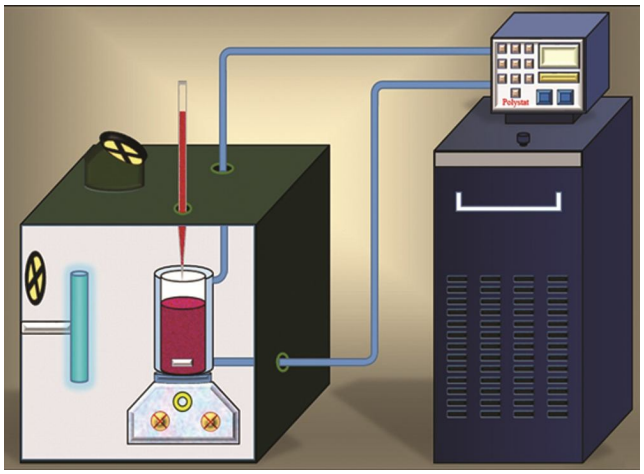

Fig. 4 — Schematic diagram of the photocatalytic reactor system.

$$\text{Efficiency} = \frac{(C_0 - C_e)}{C_0} \times 100 \quad ...(1)$$

where C_0 is the original dye concentration and C_e is the equilibrium concentration, mg/L. The amount of dye molecules adsorbed per unit weight of adsorbent, q_e (mg/g) is calculated using the subsequent expression:

$$q_e = \frac{C_0 - C_e}{w \times V} \quad ...(2)$$

where C_0 and C_e (mg/L) are same as in (Eq. (1)), V(mL) is the volume of dye solution, and w (mg) is the weight of adsorbent.

Results and Discussion

Physicochemical characterization of ZnO-Ghezeljehnanoclay composite

The acquired nanocomposite was characterized by FT-IR, SEM-EDS, and zeta potential measurement. Fig. 2(m) and Fig. 3(c) show FT-IR spectra nanocomposite measured in range 450-4000 cm^{-1} before and after dye adsorption. The existence of a band at 467 cm^{-1}approves the synthesis of ZnO because it is the individual absorption band for the Zn–O stretching vibration. The presence of ZnO in the prepared ZnO-nanoclay composite was checked by EDS analysis (Fig. 2n). The surface morphological structure of *Ghezeljeh* nanoclay and ZnO-*Ghezeljeh* nanoclay composite at *p*H 2 before and after BV16 dye adsorption was identified by SEM (Fig. 2a-d). A smoother surface of nanoclay and nanocomposite after the adsorption process was renowned. The dye molecules seem to have designed a void-free film covering the reliefs of particles and porosity of the aggregates. In contrast, the clay before adsorption shows well discernable particles and a porous structure[41]. The zeta potential of the particles was achieved (Table 2).

Absorption spectrum and photocatalytic discoloration of cationic dye Basic Violet 16 (BV16)

The results showed fast BV16 adsorption in just two minutes and gradually became slower as equilibrium position was approached. Numerous and free active surface sites of the adsorbent were accessible at the initial step of the reaction, and as the time lapsed, the free sites reduced in number consequently slowing down the adsorption process. This fast reaction suggests the strong electrostatic interaction between the negatively charged surface and the dye cations. The adsorption and photocatalytic degradation efficiencies of BV16 on *ZnO-Ghezeljeh nanoclay composite* were evaluated by determining the percentage decrease of the absorbance at 548 nm. The temporal absorption spectral changes during the photocatalytic degradation of Basic Violet 16 in irradiated aqueous ZnO-*Ghezeljeh* nanoclay composite suspension are exhibited in Fig. 5. The UV-vis absorption of Basic Violet 16 is characterized by one band in the visible region, with its maxima located at 548 nm and by three bands at 233, 298, and 364 nm. The disappearance of the ultraviolet and visible bands indicates that dye was successfully destroyed during the treatment. The Basic Violet 16 is a cationic dye and all tested minerals were negatively charged, complete adsorption was expected. No Basic Violet 16 remained in solution (250 mL charged with 120 mg/L BV16 and 0.1 g adsorbent), approving complete adsorption of the dye. While samples were exposed to direct UV light, the absorption spectrum photodegradation of the free dye was measured at 10 min intervals.

Effect of *p*H on decolo rization rate

The wastewater from dye manufacturing commonly has a various range of *p*H values. *p*H plays a critical duty both in the characteristics of dye wastes and in the generation of hydroxyl radicals. Also, it can affect at the equivalent time the surface charge of the adsorbent, the ionization amount of functional groups of the adsorbate, besides the mechanism of adsorption[42]. Consequently, the influence of *p*H in the degradation of dyes by UV irradiation was investigated. The experiments were carried out with a dye concentration of 200 mg/L, and 0.1 g ZnO-*Ghezeljeh* nanoclay composite at *p*H 2, 3, 5, and 9 for 290 min. The *p*H of the solution is adjusted before irradiation and it is not measured during the reaction. Fig. 6A demonstrates adsorption and photocatalytic

Table 2 — The Zeta potential measurements of the particles

Sample	Dielectric Constant	Electric Field (V/cm)	Mean Mobility (μm/s/V/cm)	Mean Zeta Potential (mV(T=21.31^{0}C))
Ghezeljeh nanoclay	79.810	6.940	-1.880	-25.970(pH=5.64)
ZnO-*Ghezeljeh* nanoclay composite	79.750	7.470	-0.940	-12.910(pH=6.62)

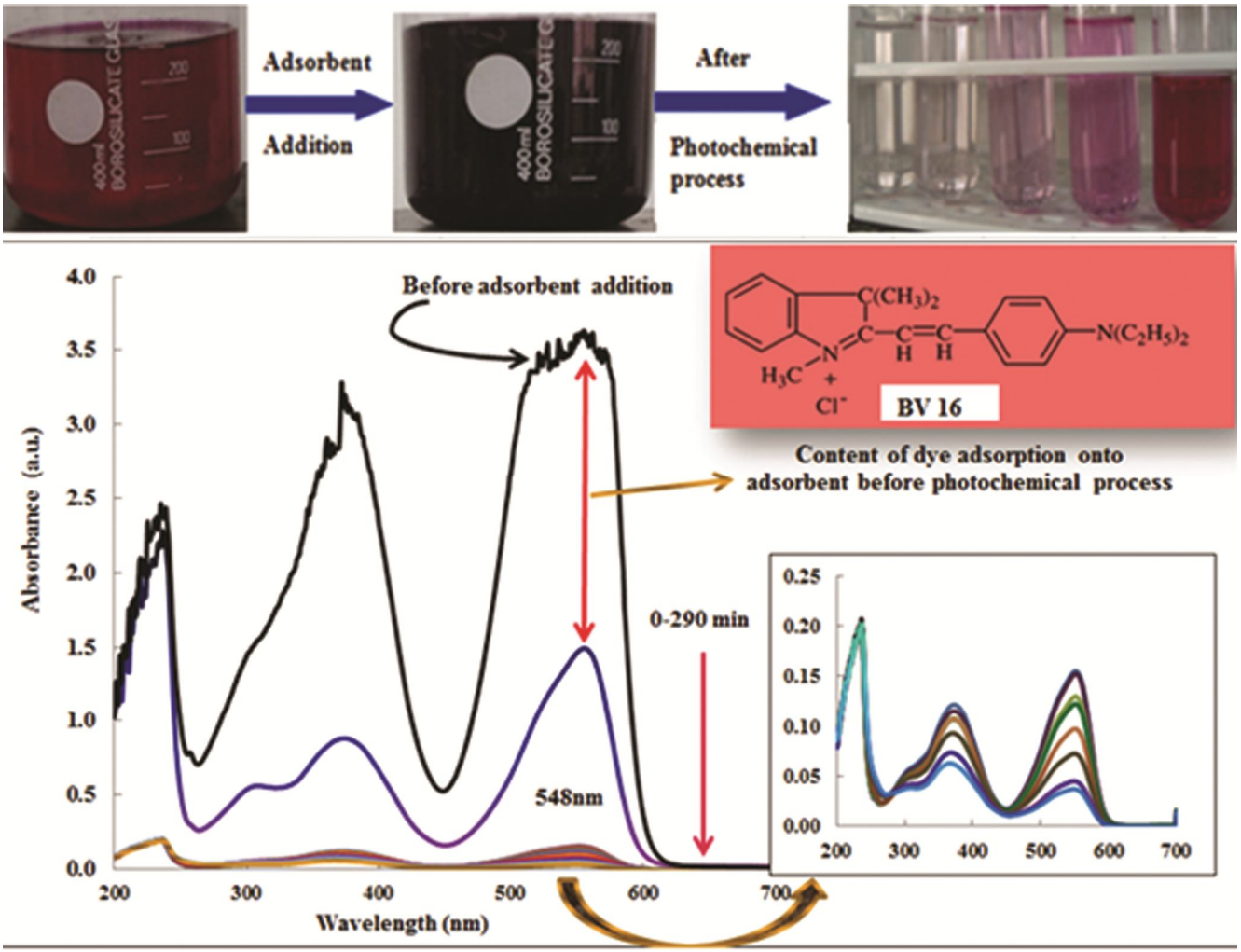

Fig. 5 — The UV–visible spectra of BV16 at different irradiation times (experimental conditions: *p*H of dye solution: 2, temperature: 25^0C, stirring speed: 750 rpm, amount of ZnO-natural *Ghezeljeh* nanoclay composite: 0.1 g, total volume: 250 mL, dye concentration: 200 mg/L).

degradation of BV16 at different *p*H values. The maximum adsorption and photocatalytic degradation (58.70% and 97.36%, respectively) arehigh in acidic medium (at *p*H 2 after 290 min of UV irradiation), and decreases with the increase in *p*H of the dye solution.

Effect of initial dye concentration

The influence of initial dye concentration on the decolorization (adsorption and photocatalytic degradation) efficiency and the correlation between the adsorption capacity (q_e) and initial dye concentration at different temperatures were surveyed by varing the initial concentration from 150 to 250 mg/L at constant conditions (0.1 g nanocomposite at solution *p*H 2) and results are shown in Fig. 6B and D. As seen in the figures, decolorization efficiency is inversely affected by dye concentration. At low initial dye concentration, adsorption of dye onto nanocomposite reaches equilibrium very hastily, however, when initial concentration rise, more materials are adsorbed on the surface of nanocomposite. Thus, there are only a fewer active sites for adsorption of hydroxyl ions accordingly the generation of hydroxyl radicals will be reduced. Additional, as the concentration of dye solution rise, the photons get captured beforehand they can reach the nanocomposite surface, hence the adsorption of photons by the nanocomposite declines, and then the degradation percent is reduced[43].

Effect of nanocomposite amount

The effect of adsorbent amount on dye elimination was investigated by contacting 250 mL of dye

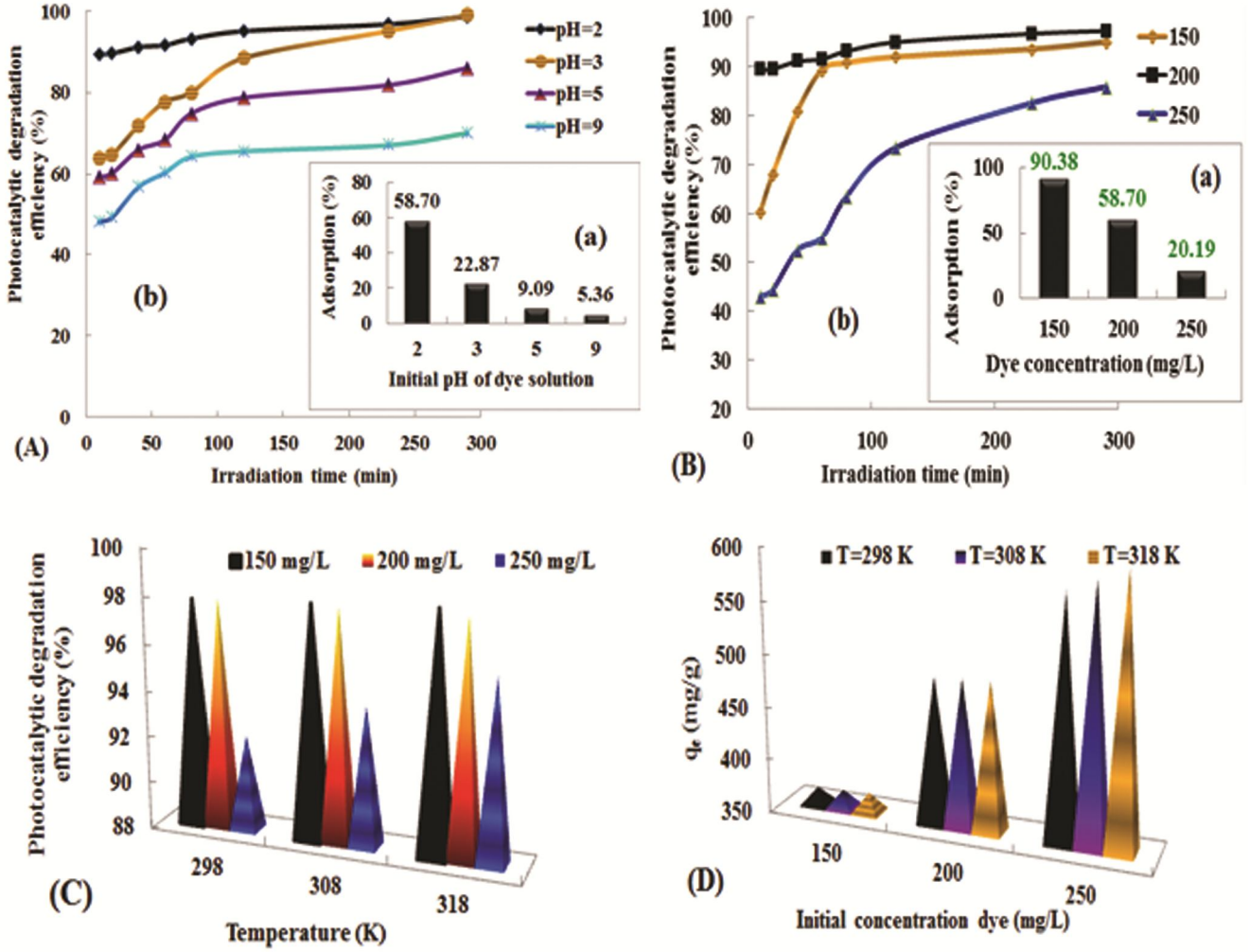

Fig. 6 — Effect of initial (A) *p*H; (B) dye concentration of BV16 on the (a) adsorption (b) photocatalytic degradation efficiency; (C) Effect of different temperatures on decolorization efficiency BV16; (D) Effect of initial dye concentration of BV16 on the adsorption capacity at different temperatures (stirring speed: 750 rpm, amount of ZnO-*Ghezeljeh*nanoclay composite: 0.1 g, total volume: 250 mL)

solution with initial dye concentration of 200 mg/L at *p*H 2 at room temperature for 290 min and the results are illustrated in Fig. 7A. The dye degradation increases with increasing catalyst concentration, which is representative of heterogeneous photocatalysis. The increase in catalyst quantity principally increases the number of active sites on the photocatalyst surface therefore causing an increase in the number of $^{\bullet}OH$ radicals which can play in real discoloration of dye solution. Further than a certain limit of catalyst quantity, the solution becomes unclear and thus blocks UV radiation for the reaction to enhancement and thus percentage degradation starts declining[44].Adsorbent amount of 0.1 g was found to lead to the highest photocatalyst degradation. This value was used in the remaining experimentations.

Effect of salt addition

The wastewaters from textile-manufacturing or dye-producing activities have diverse categories of suspended and dissolved compounds such as acids, alkalis, salts, surfactants, metal ions, etc. For this reason,the effect of ionic strength on dye exclusion efficiency was examined using NaCl, KCl, Na_2CO_3, and KI solutions of 0.1 mol/L, a dye concentration of 200 mg/L at *p*H 2 and 0.1 gZnO-*Ghezeljeh* nanoclay composite for 290 min. It can be seen in Fig. 7B, the decolorization process of BV16 was more influenced by this salts. The efficiency of adsorption increased from 58.70% to 82.54% and 84.50% in the presence of KI and NaCl, respectively. The adsorption of BV16 decreased significantly in the presence of KCl (18.52%) and Na_2CO_3 (22.83%). The photocatalytic degradation efficiency of BV16

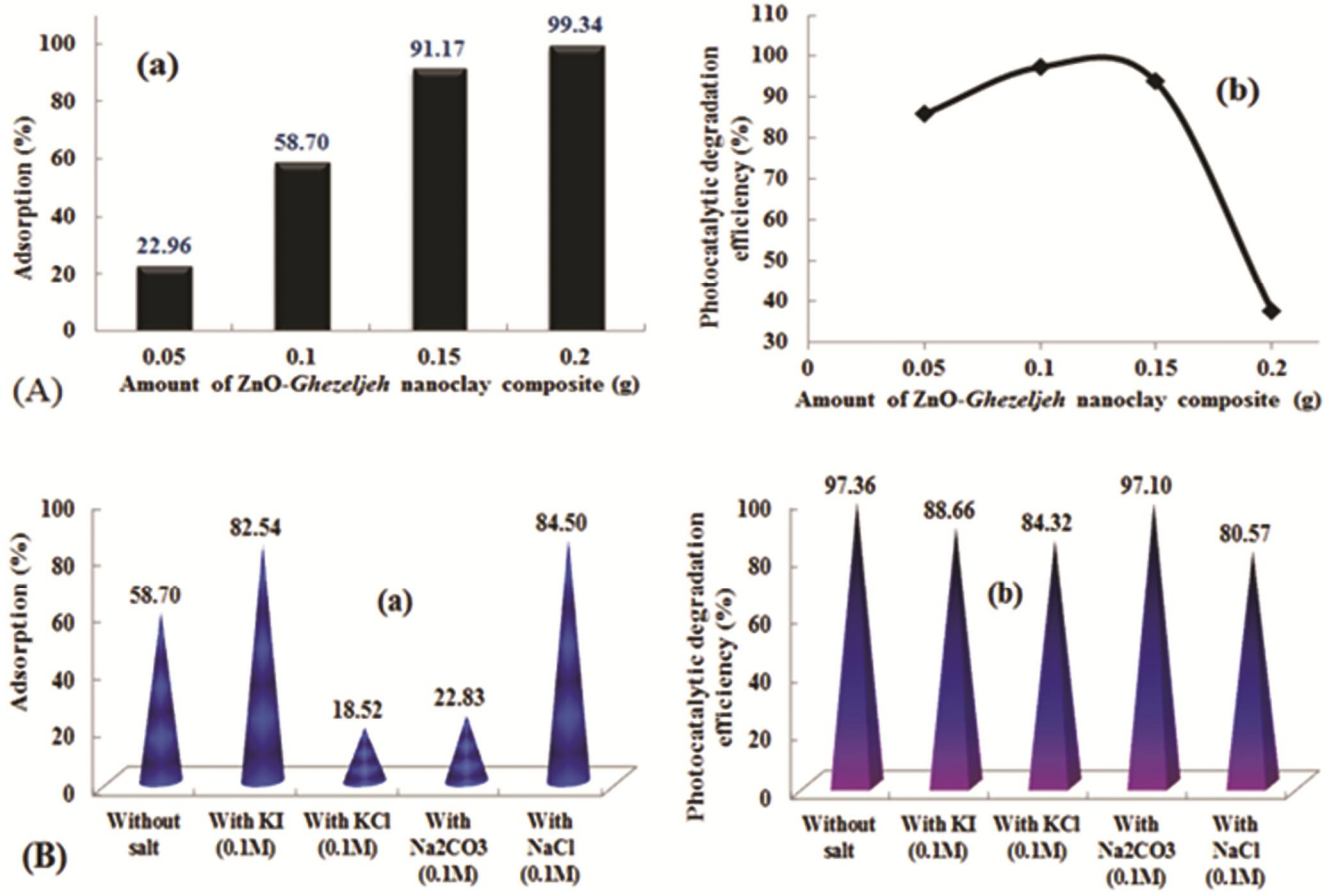

Fig. 7 — Effect of (A) nanocomposite amount, (B) salt addition on the (a) adsorption (b) photocatalytic degradation efficiency BV16 (temperature: 25^{0}C, stirring speed: 750 rpm, total volume: 250 mL, dye concentration: 200 mg/L, irradiation time: 290min, *p*H of dye solution: 2).

decreased slightlywhen compared with the absence of salts.

Effect of temperature

The effect of temperature on photocatalytic degradation process of BV16 by ZnO-*Ghezeljeh* nanoclay composite was investigated at a range of 25°C to 45°C after 290 min of UV irradiation and 0.1 g ZnO-*Ghezeljeh* nanoclay composite with the initial dye concentration of 150 mg/L, 200 mg/L, and 250 mg/L. The results of the investigate are shown in Fig. 6C. According to Fig. 6, increasing in temperature resulted in improvement of the dye degradation efficiency. On the basis of these results, the photocatalytic degradation procedure might be an endothermic occurrence.

Adsorption isotherm

At constant temperature, Adsorption isotherm shows the relationship between the adsorption capacity (q_e) and the equilibrium concentration (C_e) of dye molecules in the liquid phase. Adsorption isotherm models are commonly applied for fitting the data, and provide essential information about the mechanism of adsorption and assist us in the design of new adsorbing systems[45]. In this research, the isotherm data was evaluated using the Langmuir, Freundlich, Temkin, and Dubinin–Raduskevich equations.

Langmuir isotherm

Langmuir isotherm is regularly used to define adsorption of solute from liquid solutions and this model supposes the monolayer coverage of the adsorption surface with limited quantity of equal surface sites are energetically and showed by the subsequent equation.

$$\frac{C_e}{q_e} = \frac{1}{K_L q_m} + \frac{C_e}{q_m} \quad ...(3)$$

Values of q_m and K_L are assigned from a plot of (C_e/q_e) vs. (C_e). C_e is the equilibrium concentration of dye molecules on the adsorbent (mg/L), q_e is the quantity of dye molecules adsorbed per unit mass of adsorbent at equilibrium concentration (mg/g), q_m (mg/g) is the maximum adsorption capacity, and K_L is Langmuir constant which is related to sorption energy; precisely, K_L illustrations adsorption enthalpy which mostly differs with temperature[46]. The Langmuir isotherm was used to our experimental data and the results are presented in Table 3. One of the critical parameters of Langmuir equation is the equilibrium parameter or separation factor (R_L) (Fig. 8A). R_L can be studied by the subsequent equation:

$$R_L = \frac{1}{1+K_L C_0} \quad ...(4)$$

where C_0 (mg/L) is the highest preliminary solute concentration. The R_L shows the type of isotherm to be satisfactory ($0<R_L<1$) or unfavorable ($R_L>1$) or irreversible ($R_L=0$)[47]. This parameter showed that ZnO-*Ghezeljeh* nanoclay composite is an appropriate adsorbent for the adsorption of BV16 dye from aqueous solutions.

Freundlich isotherm

The Freundlich isotherm model supposes that the surface is heterogeneous and the energy of sorption is not constant. This model moreover supposes the multilayer adsorption. It is an empirical equation appropriate for high and middle range of solute concentration but not for low concentrations. The linear formula of the Freundlich equation is identified in the next equation[48].

$$\log q_e = \log K_F + \frac{1}{n}\log C_e \quad ...(5)$$

where q_e expresses the quantity of dye molecules adsorbed at equilibrium in mg/g, C_e is the solute equilibrium concentration in mg/L, K_F and n are Freundlich constants correlated with the adsorption capacity and intensity of adsorption, respectively (Table 3). The $\frac{1}{n}$ values show the type of isotherm to be irreversible ($\frac{1}{n}=0$), satisfactory ($0<\frac{1}{n}<1$) and unfavorable ($\frac{1}{n}>1$).

Dubinin–Radushkevich isotherm

The Dubinin–Radushkevich isotherm is further common than Langmuir's since it does not suppose a uniform surface or constant sorption potential. It is used to discriminate between the physical and chemical adsorption of dye molecules on surfaces[46]. The Dubinin–Radushkevich equation is specified by Eq. (6):

$$\ln q_e = \ln q_m - k\varepsilon^2 \quad ...(6)$$

where q_e and q_m have the same meaning as earlier, k (mol^2/J^2) is a constant correlated with the adsorption energy, and ε is the maximum adsorption capacity given by Eq.(7):

$$\varepsilon = RT\ln\left(1+\frac{1}{C_e}\right) \quad ...(7)$$

R (J/molK) is the gas constant, and T (K) is the absolute temperature (Table 4).

Temkin Isotherm

Temkin isotherm, studies the effects of the temperature of adsorption that declines linearly with coverage of the adsorbate and adsorbent interactions[49]. The Temkin isotherm has been definite in the formula as follows:

$$q_e = \frac{RT}{b}\ln\left(K_T C_e\right) \quad ... (8)$$

$$q_e = A + B\ln C_e \quad ...(9)$$

$$A = \frac{RT}{b}\ln K_T \quad ...(10)$$

Table 3 — Langmuir and Freundlich isotherm parameters for BV16 dye in photocatalytic degradation process onto ZnO-*Ghezeljeh*nanoclay composite

Temperature(K)	Langmuir constants						Freundlich constants		
	C_0(mg/L)	q_e(mg/g)	K_L(L/mg)	q_m(mg/g)	R^2	R_L	K_F(mg/g)	1/n	R^2
298	150, 200, 250	366.75, 489.17, 575.31	0.552	625	0.996	0.012 ,0.009, 0.007	320.84	0.202	0.734
308	150, 200, 250	367.50, 489.45, 586.87	0.500	666	0.995	0.013, 0.009, 0.008	306.12	0.248	0.810
318	150, 200, 250	368.28, 489.68, 597.94	0.424	715	0.995	0.015, 0.012, 0.009	283.85	0.324	0.902

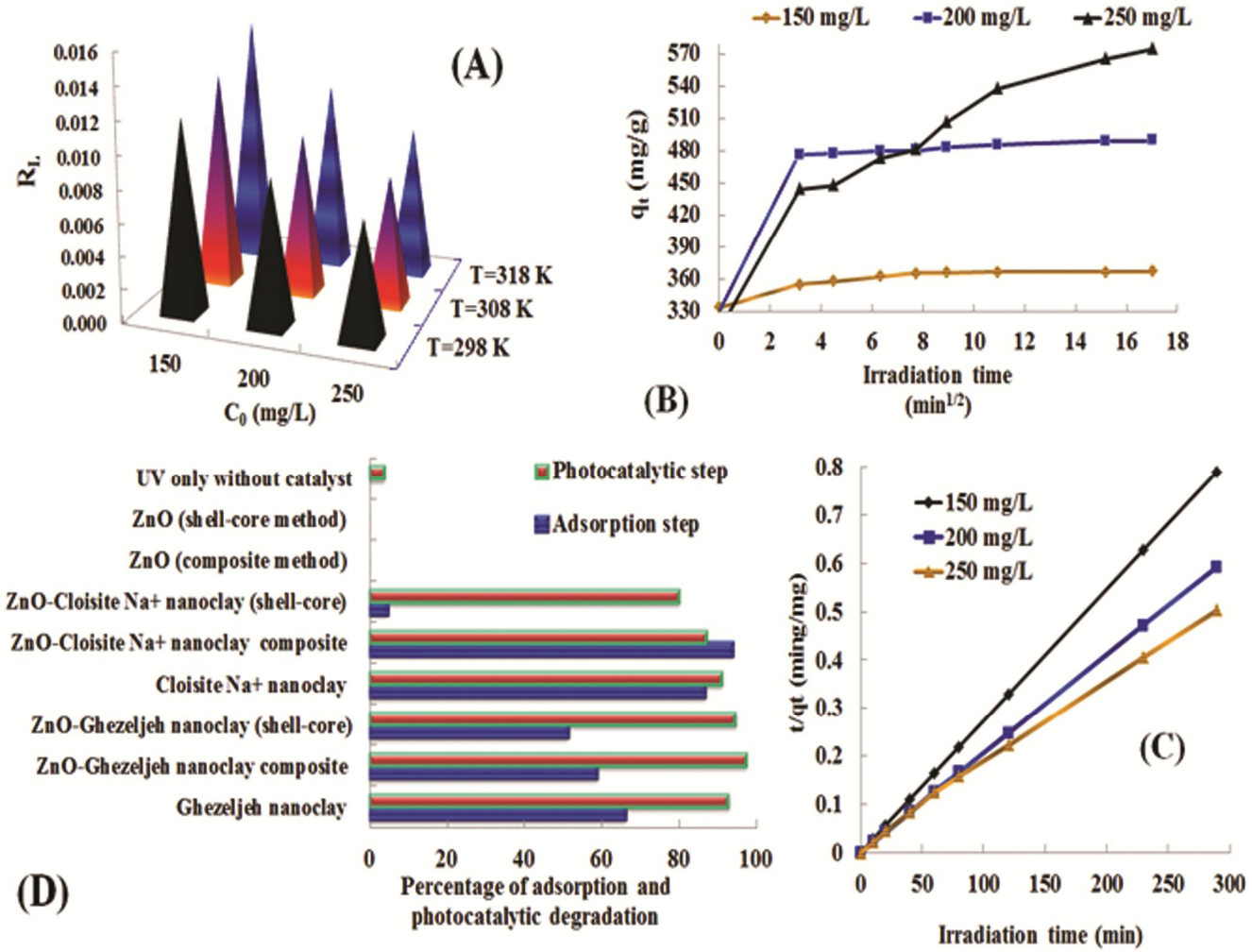

Fig. 8 — (A) Effect of Separation factor; (B) Intraparticle diffusion, (C) Pseudo second order kinetic model for BV16 dye in photocatalytic degradation process onto ZnO-*Ghezeljeh* nanoclay composite, and (D) Comparison of percentage of adsorption and photocatalytic degradation of different adsorbents (stirring speed: 750 rpm, *p*H of dye solution: 2, amount of adsorbent: 0.1g, total volume: 250 mL, dye concentration: 200 mg/L, temperature: 25^0C)

Table 4 — Dubinin-Radushkevich and Temkin isotherm parameters for BV16 dye in photocatalytic degradation process onto ZnO-*Ghezeljeh*nanoclay composite

Temperature(K)	Dubinin-Radushkevich constant				Temkin constants		
	$k(mol^2/J)$	q_m	E(J/mol)	R^2	K_{Te} (L/g)	b_{Te}(J/mol)	R^2
298	0.882	287.838	0.753	0.925	21.999	25.832	0.784
308	1.082	1047.959	0.679	0.976	9.992	21.581	0.857
318	1.331	5272.711	0.613	0.999	4.563	16.962	0.938

where $B = \frac{RT}{b}$, R is gas constant (8.314 J/molK), T is the temperature (K), K_T is equilibrium binding constant (L/g); b is correlated with heat of adsorption (J/mol). The sorption data can be evaluated by Eq. (9) (Table 4).

The R^2 values expression that the dye elimination isotherm using nanocomposite obeys the Langmuir isotherm at usual temperature and Dubinin–Radushkevich isotherm at higher temperature (Tables 3 and 4).

Adsorption kinetics

In order to estimate the kinetic mechanism of BV16 dye in photocatalytic degradation evolution onto ZnO-*Ghezeljeh* nanoclay composite, specific constants of sorption were assigned using pseudo-

first-order, pseudo-second-order, and intraparticle diffusion[50]. Pseudo-first-order model usually revealed as follows:

$$\log(q_e - q_t) = \log q_e - \frac{k_1 t}{2.303} \quad \ldots(11)$$

where q_e is the quantity of dye molecules adsorbed per unit weight of adsorbent at equilibrium i.e., adsorption capacity (mg/g), qt is the quantity of adsorbent adsorbed (mg/g) at any time t and k_1 is the rate constant (Table 5).

Pseudo-second-order rate model is known as follows:

$$\frac{t}{q_t} = \frac{1}{k_2 q_e^2} + \frac{t}{q_e} \quad \ldots(12)$$

where k_2 is the rate constant. The values of k_2 can be assigned from the plot of $\frac{t}{q_t}$ versus t; see Fig. 8C, and Table 5. To define the rate-controlling stage, intraparticle diffusion model was employed to adsorption kinetic data as is known by the next equation.

$$q_t = k_{int} t^{\frac{1}{2}} \quad \ldots(13)$$

where q_t is the quantity of metal ions adsorbed onto ZnO-*Ghezeljeh* nanoclay composite at time t, and k_{int} is the rate constant for intraparticle diffusion. Fig. 8B shows a plot of q_t vs. $t^{1/2}$. It may present multi-linearity which shows two or more stages happening in the photocatalytic degradation progression. The first sharper section ($t \leq 10$ min) is the outside surface adsorption or rapid adsorption stage. The second section (t=10 to t=60 min) is the slow adsorption stage where the intraparticle diffusion rate is checked. The third (t>60 min) is the finishing equilibrium stage where intraparticle diffusion starts to reduce speed due to enormously low solute concentration in the solution. The parameters calculated are given in Table 5. The value of k_{int} was greater at the higher concentrations. The intraparticle diffusion is not the only rate controlling step, but also other kinetic models may control the rate of adsorption, all of which may possibly be effective simultaneously. The linearity of the plots (R^2) reveals that pseudo-second order kinetic model show a important role in the uptake of the dye.

Determination of thermodynamic parameters

Three thermodynamic factors,free energy change (ΔG^0) enthalpy change (ΔH^0) and entropy change (ΔS^0) were assigned by the next equations:

$$k_L = \frac{q_e}{C_e} \quad \ldots(14)$$

$$\Delta G^0 = -RT \ln k_L \quad \ldots(15)$$

$$\ln k_L = \frac{\Delta S^0}{R} - \frac{\Delta H^0}{RT} \quad \ldots(16)$$

$$\Delta S^0 = \frac{\Delta H^0 - \Delta G^0}{T} \quad \ldots(17)$$

where R is the universal gas constant, 8.314 J/molK; T is the absolute temperature (K), and k_L is the Langmuir constant (mol/L). ΔS^0 and ΔH^0 could be achieved from the slope and intercept $\ln k_L$ versus 1/T according to the equation (16). Values of ΔS^0, ΔH^0 and ΔG^0 are presented in Table 6. Physical and chemical adsorptions are discerned from the amount of the free energy of adsorption. The change in free energy (ΔG^0) for physisorption is between −20 and 0 kJ/mol, but chemisorption is in a range of −80 to −400 kJ/mol. The values of ΔG^0 attained in this research in the ranges of −20 and 0 kJ/mol, are proposing a physical adsorption progression improved by electrostatic effect. The negative values of ΔG^0 approve the achiev ability and spontaneous nature of the procedure. The positive values of ΔH^0 show the existence of an energy obstruction in the adsorption procedure. Furthermore, the positive values of entropy change (ΔS^0) show that the randomness at the solid–liquid boundary throughout the photocatalytic degradation procedurerises[49-52].

Table 5 — Adsorption kinetics models and intraparticle diffusion model parameters for BV16 dye in photocatalytic degradation process onto ZnO-*Ghezeljeh* nanoclay composite

C_0(mg/L)	Pseudo first order kinetic model			Pseudo second order kinetic model			Intraparticle diffusion	
	K_1	q_e(mg/g)	R^2	K_2	q_e(mg/g)	R^2	K_{int}(mg/gmin$^{1/2}$)	R^2
150	0.017	11.564	0.789	0.0073	370.370	1	2.250	0.999(t=10 to t=60 min)
200	0.016	29.060	0.799	0.0028	500	1	0.879	0.954(t=10 to t=60min)
250	0.013	186.122	0.970	0.0002	588.235	0.998	8.791	0.954(t=10 to t=60min)

Table 6 — Thermodynamic parameters for BV16 dye in photocatalytic degradation process onto ZnO-*Ghezeljeh* nanoclay composite

C_0 (mg/L)	Temperature (K)	ΔS^0 (kJ/molK)	ΔH^0 (kJ/mol)	ΔG^0 (kJ/mol)
	298	0.067	8.279	-11.672
150	308			-12.314
	318			-13.012
	298	0.046	1.949	-11.712
200	308			-12.173
	318			-12.629
	298	0.113	25.417	-8.338
250	308			-9.347
	318			-10.607

Photodegradability

In this research, we studied whether adsorption of BV16 to different clays might inhibit its photodegradation. The photocatalytic decolorization of BV16 dye in aqueous ZnO-natural *Ghezeljeh* nanoclay composite suspension, compared to the performance of the dye on *Ghezeljeh* nanoclay lone, ZnO-*Ghezeljeh* nanoclay (shell-core), Cloisite Na^+ nanoclay lone, ZnO-Cloisite Na^+ nanoclay composite, ZnO-Cloisite Na^+ nanoclay (shell-core), ZnO catalyst individual (by using the manner that be defined in synthesis section, was synthesized). The results are offered in Fig. 8D and Fig. 2. When the dye, absent catalysts,was irradiated (UV lone) there was slight degradation (3.65%) and in the presence of only prepared ZnO catalyst, 0% decolorization of BV16 was observed.

Conclusion

In the present study, ZnO-natural *Ghezeljeh* nanoclay composite, ZnO-*Ghezeljeh* nanoclay (shell-core), ZnO-Cloisite Na^+ nanoclay composite, ZnO-Cloisite Na^+ nanoclay (shell-core), and ZnO catalyst individual (composite and shell-core methods) have been synthesized and their dye exclusion abilities were investigated. Cationic dye Basic Violet 16 (BV16) is used as model compounds. For this purpose, numerals of parameters are optimized: quantity of adsorbent, *p*H of the dye solutions, contact time, ionic strength, adsorbate medium temperature, and preliminary dye concentration. Although *Ghezeljeh* nanoclay in pure and natural form display a cationic exchange capacity, experiences verify a worthy ability throughout the photocatalytic reaction cationic dye molecules (BV16); consequently, a combination of *Ghezeljeh* nanoclay and ZnO creates photooxidation effective for the elimination of dye compounds from wastewater. The results moreover specified that in the photocatalytic degradation of BV16 dye, adsorption of dye to catalyts is one of the significant factors which define the degradation rate. The maximum adsorption and photocatalytic degradation are great in acidic medium, and elevation in temperature caused in heightening of the dye degradation efficiency. The efficiency of adsorption improved from 58.70% to 82.54% and 84.50% in the existence of KI and NaCl, respectively. The adsorption of BV16 reduced meaningfully in the existence of KCl (18.52%) and Na_2CO_3 (22.83%). The photocatalytic degradation efficiency of BV16 lessened faintly when compared with the lack of salts. Kinetic data discovered that the intraparticle diffusion is not the individual rate controlling stage, but also other kinetic models can manage the rate of adsorption, all of which can be employed at the same time. The linearity of the plots (R^2) reveals that pseudo-second order kinetic model show an important character in the uptake of the dye. The R^2 values display that the dye elimination isotherm using nanocomposite follows the Langmuir isotherm at usual temperature and Dubinin–Radushkevich isotherm at greater temperature. The values of ΔG^0 attained in this research are proposing a physical adsorption procedure. The negative values of ΔG^0 approve the practicability and involuntary nature of the process. The positive values of ΔH^0 show the existence of an energy obstruction in the adsorption procedure. Furthermore, the positive values of entropy change (ΔS^0) specify that the arbitrariness at the solid–liquid boundary throughout the photocatalytic degradation procedurerises.

Acknowledgement

The authors are grateful for the financial support of this work by the Imam Khomeini International University (IKIU), and Mines and Mining Industries Development and Renovation Organization of Iran (IMIDRO).

References

1 Kalapriya K & Gurumallesh Prabu H, *Int J Recent Sci Res*, 3(8) (2012) 670.
2 Rahmani Z, Kermani M, Gholami M, Jonidi Jafari A & Mahmoodi N M, *Iran J Environ Health Sci Eng*, 9 (2012) 14.
3 Daneshvar N, Salari D & Khataee A R, *J Photochem Photobiol A: Chem*, 162 (2004) 317.
4 Gogate P R & Pandit A B, *Adv Environ Res*, 8 (2004) 501.
5 Gogate P R & Pandit A B, *Adv Environ Res*, 8 (2004) 553.

6 Yassıtepe E, Yatmaz H C, Ozturk C, Ozturk K & Duran C, *J Photochem Photobiol A: Chem*, 198 (2008) 1.
7 Augugliaro V, Litter M, Palmisano L & Soria J, *Photochem Photobiol C: Photochem Rev*, 7 (2006) 127.
8 Behnajady M A, Modirshahla N & Hamzavi R, *J Hazard Mater*, 133 (2006) 226.
9 Daneshvar N, Aber S, Seyed Dorraji M S, Khataee A R & Rasoulifard M H, *Sep Purif Technol*, 58 (2007) 91.
10 Daneshvar N, Rasoulifard M H, Khataee A R & Rasoulifat M H, *J Hazard Mater*, 43 (1–2) (2007) 95.
11 Lizama C, Freer J, Baeza J & Mansilla H, *Catal Today*, 76 (2002) 235.
12 Mihai G D, Meynen V, Mertens M, Bilba N, Cool P & Vansant E F, *J Mater Sci*, 45 (21) (2010) 5786.
13 Byrappa K, Subramani A K, Ananda S, Rai K M, Sunitha M H, Basavalingu B & Soga K, *J Mater Sci*, 41 (2006) 1355.
14 Jeon H J, Chung Y, Kim S Y, Yoon C S & Kim Y H, *Mater Sci Fo*r, (1145–1148) (2004) 449.
15 Silvestre-Albero J, Serrano-Ruiz J C, Sepu´lveda-Escribano A & Rodrı´guez-Reinoso F, *Appl Catal A*, 351 (2008) 16.
16 Zhai J, Tao X, Pu Y, Fei Zeng X & Chen J F, *Appl Surf Sci*, 257 (2) (2010) 393.
17 Zhi Y, Li Y, Zhang Q & Wang H, *Langmuir*, 26 (19) (2010) 15546.
18 Baruah S, Sinha S S, Ghosh B, Pal S K, Raychaudhui A K & Dutta J, *J Appl Phys*, 105 (2009) 074308-1.
19 Viswanatha R, Sapra S, Satpati B, Satyam P V, Dev B N & Sarma D D, *J Mater Chem*, 14 (2004) 661.
20 Fatimah I, Wang S &Wulandari D, *Appl Clay Sci*, 53 (2011) 553.
21 Auta M & Hameed B H, *Chem Eng J*, 198 (2012) 219.
22 Liu P & Zhang L, *Sep Purif Technol*, 58 (1) (2007) 32.
23 Tahir S S & Rauf N, *Chemosphere*, 63 (2006) 1842.
24 Chong M N, Jin B, Chow C W K & Saint C, *Water Res*, 44 (2010) 2997.
25 Errais E, Duplay J, Darragi F, M´Rabet I, Aubert A, Huber F & Morvan G, *Desalination*, 275 (2011) 74.
26 Meshram S, Limaye R, Ghodke S, Nigam S, Sonawane S & Chikate R, *Chem Eng J*, 172 (2011) 1008.
27 Hardy R G & Tucker, Techniques in Sedimentology, edited by ME Tucker (Blackwell Scientific publishing, Oxford, New York), 1988, pp. 191.
28 Soleimani M, Rafiei B & Hassanzadeh Siahpoosh Z, *J Anal Chem*, 70 (7) (2015) 794.
29 Soleimani M & Hassanzadeh Siahpoosh Z, *Chin J Chem Engin*, 23 (2015) 1819.
30 Soleimani M & Hassanzadeh Siahpoosh Z, *Anal Bioanal Chem Res*, 3(2) (2016) 195.
31 Soleimani M & HassanzadehSiahpoosh Z, *J Appl Chem Res*, Special issue(2015) 7.
32 Novakovi´c T, Ro˘zi´c L, Petrovi´c S & Rosi´ A, *Chem Eng J*, 137 (2008) 436.
33 Tyagi B, Chudasama C D & Jasra R V, *Spectrochim Acta A*, 64 (2006) 273.
34 Hang X, Tianlong Y & Junfeng L, *Mater Lett*, 117 (2014) 263.
35 van Olphen H & Fripiat J J, *Data Handbook for Clay Materials and other Nonmetallic Minerals*, (Pergamon Press, New York), 1979.
36 Meier L P & Kahr R, *Clays Clay Miner*,47 (1999) 386.
37 Amman L, Bergaya F & Lagaly G, *Clay Miner*, 40 (2005) 441.
38 Grim R E, *Clay Mineralogy*, (McGraw-Hill, New York), 1968.
39 Gu X, Evans L J &Barabash S J, *Geochim Cosmochim Acta*,74 (2010) 5718.
40 Eren E & Afsin B, *J Hazard Mater*, 15 (2008) 682.
41 Elmoubarki R, Mahjoubi F Z,Tounsadi H, Moustadraf J, Abdennouri M, Zouhri A, El Albani A & Barka N, *Water ResourInd*, 9 (2014) 16.
42 Rauf M A & Salman Ashraf S, *Chem Eng J*, 151 (2009) 10.
43 Akyol A, Yatmaz H C & Bayramoglu M, *Appl Catal B: Environ*, 54 (2004) 19.
44 Ghasemi Z, Seif A, Ahmadi T S, Zargar B, Rashidi F & Rouzbahani G M, *Adv Powder Technol*, 23 (2012) 148.
45 Erdem E, Karpinar N & Donat R, *J Coll Interface Sci*, 280 (2004) 309.
46 Abbasizadeh S, Keshtkar A R & Mousavian M A, *Chem Eng J*, 22 (2013) 161.
47 Rashidi F, Sarabi R S, Ghasemi Z & Seif A, *Superlatt Microstruct*, 48 (2010) 577.
48 Djeribi R & Hamdaoui O, *Desalination*, 225 (2008) 95.
49 Sheel T & ArthobaNayaka Y, *Chem Engin J*, 191 (2012) 123.
50 Mahmoodi N M, Hayati B & Arami M, *Ind Crops Prod*, 35 (2012) 295.
51 Sheela T, ArthobaNayaka Y, Viswanatha R, Basavanna S & Venkatesha T G, *Powder Technol*, 217 (2012) 163.
52 Soleimani M & Hassanzadeh Siahpoosh Z, *J Tai Inst Chem Engin*, 59 (2016) 413.